March 22, 2004

Bilayer splitting and coherence effects in optimal and underdoped $Bi_2Sr_2CaCu_2O_8+\delta$

Y. D. Chuang
University of Colorado

A. D. Gromko
University of Colorado

A. V. Fedorov
University of Colorado

Y. Aiura
National Institute for Advanced Industrial Science and Technology

K. Oka
National Institute for Advanced Industrial Science and Technology

See next page for additional authors

Bilayer splitting and coherence effects in optimal and underdoped $Bi_2Sr_2CaCu_2O_{8+\delta}$

Y.-D. Chuang,[1,2] A. D. Gromko,[1] A. V. Fedorov,[1,2] Y. Aiura,[3] K. Oka,[3] Yoichi Ando,[4] M. Lindroos,[5,6]
R. S. Markiewicz,[5] A. Bansil,[5] and D. S. Dessau[1]

[1]*Department of Physics, University of Colorado, Boulder, Colorado 80309-0390, USA*

[2]*Advanced Light Source (ALS), Lawrence Berkeley National Laboratory, Berkeley, California 94720, USA*

[3]*National Institute for Advanced Industrial Science and Technology (AIST), AIST Tsukuba Central, 1-1-1 Umezono, Tsukuba, Ibaraki 305-8568, Japan*

[4]*Central Research Institute of Electric Power Industry (CRIEPI), 2-11-1 Iwato-Kita, Komae, Tokyo 201-8511, Japan*

[5]*Physics Department, Northeastern University, Boston, Massachusetts 02115, USA*

[6]*Tampere University of Technology, P.O. Box 692, SF-33101, Tampere, Finland*

(Received 9 January 2003; published 22 March 2004)

We have carried out extensive high-resolution angle-resolved photoemission (ARPES) experiments on $Bi_2Sr_2CaCu_2O_{8+\delta}$ samples, covering the entire doping range from the overdoped to the optimally and underdoped regimes in the normal state. Our focus is on delineating the doping dependence of the bilayer splitting which is associated with the intracell coupling of electrons between the two CuO_2 planes. We exploit the photon energy of 47 eV, where strong ARPES matrix element effects are found to provide a tremendous enhancement of the antibonding to bonding component of the bilayer split bands near $(\pi,0)$, in good agreement with the predictions of corresponding first-principles simulations. Our detailed analysis indicates that the size of the bilayer splitting is only weakly dependent on the doping level, implying that electronic excitations continue to maintain some degree of coherence even in the underdoped regime.

DOI: 10.1103/PhysRevB.69.094515 PACS number(s): 74.25.Jb, 79.60.−i

I. INTRODUCTION

The fundamental building blocks of all known high-T_c cuprate superconductors are sheets of CuO_2 planes separated by a variety of rocksalt layers, which are believed to stabilize the structure and provide carriers for doping the CuO_2 planes. The layered nature of the structure induces a large anisotropy in many physical properties, such as the in-plane to out-of-plane resistivity ratio $\rho_{a,b}/\rho_c$ and its temperature dependence $\rho_{(a,b),c}(T)$.[1,2] A central issue has been whether electrons sample the three-dimensional structure in these materials, or whether they become confined to the two-dimensional(2D) CuO_2 sheets or bilayers. In this connection, a variety of exotic scenarios such as spin-charge separation,[3] Luttinger liquid,[4] and others[5] have been proposed, where in-plane quasiparticles (coherent behavior) cease to exist as low-dimensional states are formed. It is clear that an understanding of the in-plane as well as out-of-plane coherence of electronic states in the cuprates has wide-ranging and fundamental implications.

In the generic doping phase diagram of cuprates, it has long been thought that the physics near the heavily overdoped side should mimic a normal three-dimensional Fermi liquid as correlation and confinement effects are reduced. In contrast, on the underdoped side, correlation effects are expected to grow as one approaches the undoped parent compounds, which are known to be Mott insulators. For example, strong correlations may yield the exotic pseudogapped ''non-Fermi-liquid'' ground state in the underdoped regime (for a review, see Refs. 6 and 7). These two regimes are presumably bridged by some sort of a dimensional crossover or perhaps by the intervention of a phase transition. In the former case, the 3D physics observed at high doping and/or low temperatures crosses over to a 2D correlated electron state in the underdoped regime.[8]

A significant advance was made recently by angle-resolved photoemission (ARPES) experiments on the heavily overdoped bilayer cuprates $Bi_2Sr_2CaCu_2O_{8+\delta}$ (Bi2212 or BSCCO), which showed for the first time the existence of the normal state *c*-axis intracell coupling;[9,10] see also Refs. 11 and 12. This coupling manifests itself as the splitting of a CuO_2 plane-related state near the Fermi energy E_F into a pair of bonding (B) and antibonding (A) combinations of levels associated with the CuO_2 bilayer. The observation of this splitting indicates that electronic states are coherent along the *c* axis at least to the distance between CuO_2 bilayers (3.2 Å). Although the value of the intracell coupling deduced from ARPES experiments, $t_\perp \approx 55$ meV, is smaller than band theory predictions by a factor of about 3, nevertheless, its presence is generally in accord with the expectation of a Fermi-liquid-like behavior in the overdoped system.

While there now appears to be a consensus on the existence of bilayer splitting in overdoped samples, there is much confusion about whether it exists in optimal or underdoped samples.

Primarily through a comparison of single-layer and bilayer BSCCO as well as some photon energy-dependent studies, Feng *et al.* have argued that the bilayer splitting does persist to low dopings.[15] Their data on these samples were, however, limited to the $(\pi,0)$ point of the Brillouin zone where superstructure effects are an important complication. The Dresden group has used Pb doped Bi2212 samples to remove the superstructure and also observe the bilayer splitting.[12,13] In contrast, a more recent temperature-dependent ARPES study of Bi2212 by Kaminski *et al.*[14] reports that bilayer splitting cannot be observed in overdoped samples at high temperatures (above 250 K) or in optimally doped samples in the normal state (100–350 K). They argue

that this implies the absence of both in-plane as well as out-of-plane coherence at low doping or high temperature, proposing the existence of a new phase diagram with a crossover between these two regimes. We have readdressed this issue over a wider range of k space and by exploiting the tremendous theoretically predicted selectivity of the photon-energy-dependent ARPES matrix element which accentuates different components of the bilayer split bands.[16] An important qualitative result is that we continue to observe effects of the bilayer splitting well into the underdoped regime, similar to Refs. 15,12 and 13 but in contrast to Ref. 14. In addition, we make the first estimates of the interlayer coupling parameter $t_\perp$ as a function of doping, arriving at the surprising conclusion that this parameter is roughly doping independent.

II. EXPERIMENT

High-resolution ARPES experiments were performed on the bilayer cuprate $Bi_2Sr_2CaCu_2O_{8+\delta}$ over a wide range of oxygen concentrations, which included heavily overdoped (OD, $T_c=55$ K), optimally doped (OpD, $T_c=91$ K), and underdoped (UD, $T_c=78$ K) samples. Various doping levels were achieved via high-temperature annealing: the OD samples with a T_c of 55 K were obtained by annealing as-grown crystals at $T=400\,^\circ$C under a pressurized ($\gtrsim$1000 atm) oxygen atmosphere, OpD samples with a T_c of 91 K by annealing at $T=700\,^\circ$C in air, and UD samples with a T_c of 78 K by annealing in a reduced oxygen atmosphere (argon/100 ppm oxygen) at $T=400\,^\circ$C. All transition temperatures were determined by using a superconducting quantum interference device magnetometer.

Most of the experiments were carried out at the Advanced Light Source (ALS), Berkeley, using the Scienta 200 (SES200) endstation at the undulator beamline 10.0.1., with portions performed at the Synchrotron Radiation Center, Stoughton, WI, and at the Stanford Synchrotron Radiation Laboratory, Stanford, CA. The combined photon and electron energy resolution was about 15 meV, determined by the 10–90 % width of the Fermi edge of a low-temperature gold film. The data were obtained in the angle mode with an angular resolution of $\approx\pm0.16°$; with this angle mode, the spectra within $\pm7°$ emission angle could be collected simultaneously. At 47 eV, the converted momentum resolution is $\Delta k\approx\pm0.01\pi/a$, where the lattice constant $a\approx3.85$ Å. In order to access emission from different (k_x,k_y) regions of the Brillouin zone, the analyzer was rotated along the direction perpendicular to the incoming photon beam, keeping the sample position fixed. The angle between the central axis of the analyzer and the incoming photon beam was 83° and the photon polarization was mostly in plane. All data shown in this paper have been taken in the normal state: the temperature was 80 K for OD samples and 100 K for OpD and UD samples. The original spectra were only normalized by using the spectral weight in the energy range 50–250 meV above E_F, which is expected to be isotropic.

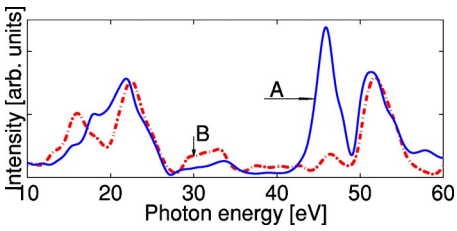

FIG. 1. (Color online) Calculated photon energy dependence of the cross sections for the bonding (B) and antibonding (A) bands at $(\pi,0)$ in tetragonal Bi2212.

III. RESULTS AND DISCUSSION

A key to resolving the bilayer splitting is to exploit the remarkable selectivity displayed by the ARPES matrix element in coupling to the individual bands as a function of the energy and polarization of the incident light, even when these bands are placed closely in energy.[16] Figure 1, which shows the computed photointensity as a function of photon energy for the bonding (B) and antibonding (A) levels (resulting from the bilayer splitting effect) at the $(\pi,0)$ (or $\bar{M}$) point in the Brillouin zone, is particularly germane in this connection. Large variations in intensity predicted between the A and B bands in Fig. 1 serve to guide the measurements in that the photon energy can be tuned to discriminate between A- and B-related features in the spectra.[17]

The ARPES work on Bi2212 has historically tended to focus on photon energies around 22 eV, although other energies are drawing an increasing interest. However, results of Fig. 1 indicate that in the 22 eV region, despite some differences, the B and A bands possess similar ARPES cross-sections. On the other hand, Fig. 1 shows that there is a special energy, namely, 47 eV, where the intrinsic intensity of the A band is very high while that of the B band is low. We have used this tremendous predicted enhancement of the A to B features at 47 eV to help deconvolute the contributions of these two bands in Bi2212, even in the underdoped samples, where the intrinsic broadening of spectral peaks tends to mask the effect of splitting.

Figure 2 shows experimental spectra as a function of momentum k_x and binding energy for three different doping levels (OD, OpD, and UD) at two different photon energies (22 eV and 47 eV). Note that k_x here refers to the $(\pi,0)-(\pi,\pi)$ line (the $\bar{M}$-$\bar{X}$ line, so that k_y is held fixed at π/a). For reference, panel (g) also shows schematic plots of the Fermi surface (FS's) associated with the B and A bands as red and black curves. False color images of the spectra are shown in panels (a)–(f), with the three left-hand panels measured with 22 eV photons and the right-hand ones with 47 eV photons. The momentum space location of these cuts is indicated by the green line in panel (g). Two sets of representative 1D cuts through the 2D spectral distributions of (a)–(f) are shown in panels (h)–(m) and give further insight into the nature of the spectra. Panels (h), (j), and (l) give intensity as a function of binding energy at $k_x=0$ [i.e., along the horizontal white lines in (a)–(f)] and are the standard energy distribution curves (EDC's) at $\bar{M}$. Panels (i), (k), and (m) give intensity as a function of k_x for zero binding energy

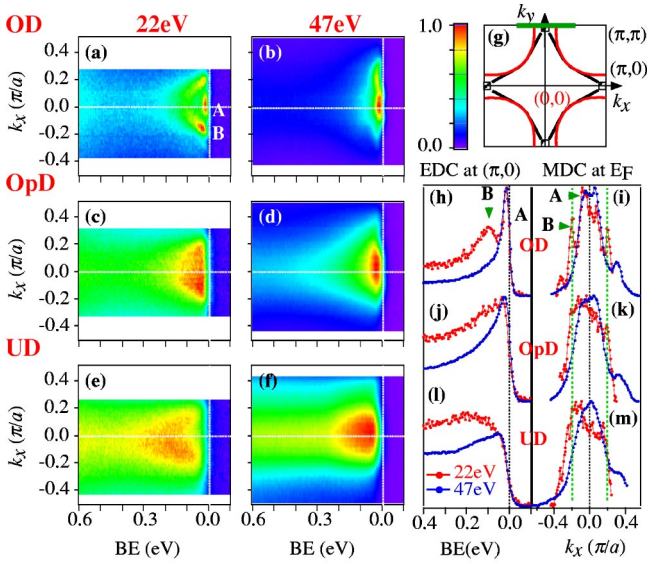

FIG. 2. (Color online) (a)–(f) ARPES spectra as a function of energy and momentum are shown with a false color intensity scale for two different photon energies (22 eV and 47 eV) and three different doping levels (OD, OpD, and UD). Momentum k_y is along the $(\pi,-\pi)$-(π,π) line. (g) A Fermi-surface plot indicating the location of the data cuts (green lines). Superlattice replica bands are not shown. Shading near $(0,\pi)$ indicates the uncertainty in locating the FS. (h),(j),(l) EDC's at the $(0,\pi)$ point, scaled such that the low binding-energy structures possess a similar intensity. (i),(k),(m) MDC's at E_F. Red curves are 22 eV data and blue curves are 47 eV data.

[i.e., along the white dashed vertical lines in (a)–(f)] and are the standard momentum distribution curves (MDC's) at E_F.

Looking at Fig. 2(a) for the OD sample at 22 eV, the presence of two bands labeled A (for antibonding) and B (for bonding) is very clear. Here, we are making the implicit assumption that these experimental A and B bands correspond to the theoretical bilayer-split A and B bands discussed in connection with Fig. 1; we will return to this point later. Consistent with the spectrum of Fig. 2(a), peaks A and B are seen in the 22 eV EDC in Fig. 2(h) (red curve). Similarly, the red MDC in panel (i) displays symmetrically placed peaks B at $k_x \approx \pm 0.2\pi/a$, and there is weight between $\approx \pm 0.1\pi/a$, which should be due to the A bands. The very flat dispersion of this band broadens these MDC peaks, with the slight asymmetry in amplitude being due to superstructure effects (to be discussed in detail later) as well as some possible matrix element effects. Additional insight is provided by the spectra at the complementary photon energy of 47 eV. As already pointed out, this photon energy is expected to enhance the A band relative to the B band. That this is indeed the case is well demonstrated for the OD sample by comparing the 22 eV and 47 eV spectra in panels (a) and (b). The 47 eV (blue curves) EDC in panel (h) as well as the MDC in panel (i) are completely dominated by the A band while the signal from the B band is barely detectable. Notably, by comparing the red and blue curves in panels (h) and (i), the line shape and the energy/momentum position of the A band is seen to be unchanged with photon energy within experimental uncertainty, though the absolute intensities are of course energy dependent due to matrix element effects. This observation is important in obtaining a unique decomposition of the spectra into contributions from A and B bands.

Turning to the OpD and UD spectra at 22 eV in Fig. 2, in contrast to the OD case, it is difficult to see the presence of two well-separated bands. The EDC's and MDC's at 22 eV (red curves) in panels (j)–(m) appear relatively featureless compared to the OD data. Nevertheless, similar to what we have observed in the OD panels (a) and (b), the 47 eV images in panel (d) and (f) show a larger concentration of spectral weight near E_F than do the 22 eV images in (c) and (e). This is seen more clearly in the EDC's in panels (j) and (l), which show a sharper and lower-energy feature at 47 eV (blue) than at 22 eV (red). These results suggest that the OpD and UD spectra may be viewed as consisting of A- and B-like components, where these features have been broadened due to various mechanisms[18] such that their intrinsic widths in energy/momentum become comparable to the scale of the bilayer splitting. If so, the 47 eV data will be expected to contain mainly the spectral weight from the A band, while the 22 eV data show additional weight from the B band inducing a strong modification of the line shape. The MDCs at E_F in panels (k) and (m) tell a similar story—the 47 eV data is more concentrated around $k_x \approx 0.0$, presumably from the A band, while the 22 eV data extends farther out in $\vec{k}$ space because it contains spectral weight from the B band as well.

Figure 3 shows integrated spectral weights over a binding-energy window of ± 10 meV around E_F over a large portion of the (k_x,k_y) plane centered at $(0,\pi)$ $(\bar{M})$. Loci of high intensity in Fig. 3 map the FS topology, effects of $\vec{k}$-dependent matrix elements notwithstanding. Panels (a)–(f) of Fig. 3 are arranged parallel to those of Fig. 2 in that the left column refers to 22 eV and the right one to 47 eV. The top, middle, and the bottom rows give data for the OD, OpD, and the UD samples, respectively. Panel (g) would help orient the reader as it indicates the (k_x,k_y) region involved in various measurements by the white box, along with schematic A and B FS's and a few of the replicas due to superlattice modulation. The black lines refer to the A FS's and red lines to the B FS's, and the associated FS replicas[19] are given by thin lines. Note that we do not close the A FS near the $(0,\pi)$ point due to an uncertainty in the direction of curvature there, and since the intensity of the A band is dominant at 47 eV, only its superlattice replicas are shown in this panel. The full set of replica FS's is shown in panel (h).

As in Fig. 2, the bilayer splitting effect is most clearly seen in panel (a) of Fig. 3 (OD, 22 eV), where we see the FS's arising from band A (overlaid with thick black curves) and band B (overlaid with thick red curves) and some of the related superstructure replicas (thin black lines). Also, similar to Fig. 2, the 47 eV data in panel (b) (OD) almost exclusively shows the FS of A band with much of the spectral weight concentrated near the $(0,\pi)$ region. In fact, our theoretical simulations indicate that the matrix elements at 47 eV favor the second zone. A comparison of panels (a) and (b) shows this effect in the experimental spectra where we see the high-intensity region in (b) shifted vertically to higher

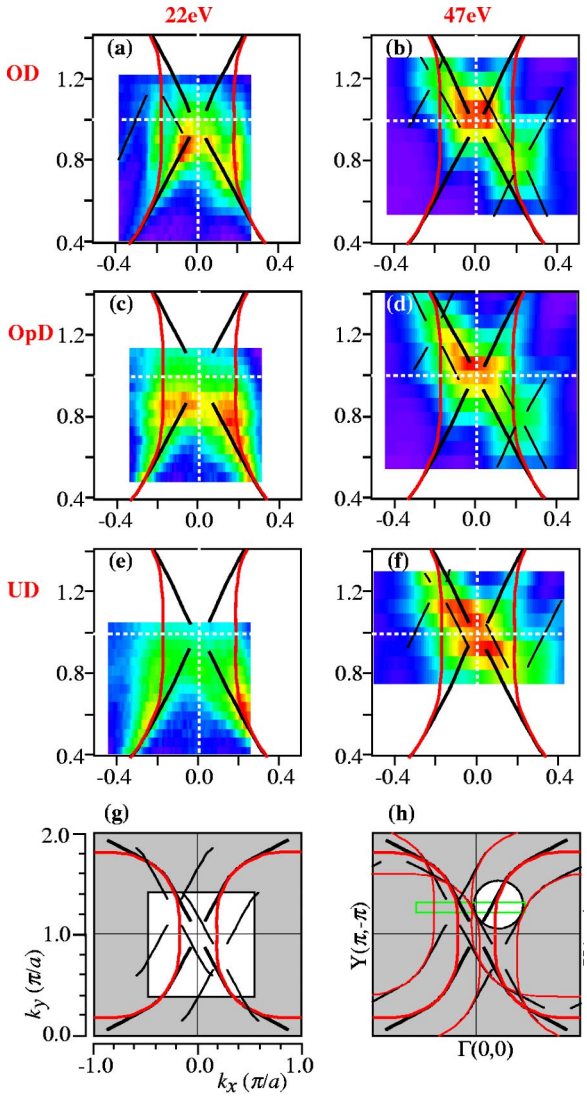

FIG. 3. (Color online) (a)–(f) Integrated spectral weight over a (−10 meV,10 meV) binding-energy window at 22 eV (left) and 47 eV (right) for three doping levels. The data boxes cover the white portion of the Brillouin zone in panel (g), which is centered around the $\bar{M}$ or $(0,\pi)$ point. In this plot, the FS from A band is shown in red and from B band in black, along with a few replica pieces of the FS. (h) Covers the same Brillouin-zone location and includes all main and first-order replica bands.

momenta above the $(0,\pi)$ point; a similar behavior also shows up in panels (d) and (f) at 47 eV, leaving aside effects of changes in the hole doping levels. On the other hand, panels (c) and (e) at 22 eV more clearly show the standard holelike FS originating from band B. We should also keep in mind that at both 22 eV and 47 eV, the secondary features arising from various modulations (superlattice, orthorhombic distortion, etc.) are observed to be relatively weak compared to the intensity of the primary features originating in the underlying tetragonal CuO_2 bands A and B. Further, they can be mostly well tracked in the experimental data.

The preceding discussion of Figs. 2 and 3 leaves little doubt that there are remarkable similarities between the OD, OpD, and UD samples, insofar as changes in spectral weights between 22 eV and 47 eV are concerned, and that these changes are in qualitative agreement with the theoretical predictions of Fig. 1.[22] These results, taken as a whole, strongly suggest that the data are well described by a common underlying mechanism at all doping levels, namely, the bilayer splitting effect. Other more exotic explanations may be possible, especially for the underdoped system, but one would argue for the simplest one in terms of the conventional bilayer splitting. If so, it follows that there must be some coherent coupling between the adjacent CuO_2 sheets even in the quite heavily underdoped samples.

Our analysis of the spectra of Figs. 2 and 3 has so far been based only on the raw data without invoking any fitting or modeling. A more quantitative determination of the bilayer splitting and the dispersion of bands A and B can however be made via a simple fitting procedure. In regions of large dispersion, MDC's tend to provide a better fit (often for bands near E_F), while in regions of slow dispersion (e.g., near the bottom of the band), the EDC's tend to be generally better suited. In any event, only those portions of the spectra should be fitted which are not close to features arising from superlattice and other effects, so that the associated contamination of the spectra is minimal.

The spectrum of the OD sample at 22 eV [Fig. 2(a)], which shows well-resolved A and B bands near the $(0,\pi)$ point, is the simplest to fit. The increased broadening of the peaks in the optimal and especially the underdoped samples can make the fitting process much more uncertain. However, we have found that, under favorable conditions of photon energy and polarization, these two bands can nevertheless be resolved for all three doping levels in certain regions of the Brillouin zone. Here we focus on a cut in the second Brillouin zone around $k_y = 1.27\pi/a$ at 47 eV, which is indicated by the green rectangular box in Fig. 3(h). This cut is interesting because it contains the region of Fig. 3(h) circled in white, which contains no replica FS's and in which the bilayer splitting should still be finite. MDC's at E_F along this cut for the three doping levels are shown in Fig. 4(a)-4(c). The left-hand side of the spectra (with negative k_x) are contaminated by superstructure bands, and were therefore not analyzed in detail. In particular, the extra intensity of this structure is due to the superposition of the main bands with multiple superstructure bands, including very high-intensity ones originating from near $(\pi,0)$. The right-hand side of the spectra, centered around $k_x \approx 0.2\pi/a$, is relatively free of such secondary effects and yet shows asymmetric peaks which cannot be fitted by a single functional form, but is well described by two Lorentzians (marked by A and B) on top of a linear background (the dotted lines). We emphasize that the ARPES matrix element displays quite strong k dependencies—see, for example, Figs. 3(a2)–3(c2) of Bansil and Lindroos.[16] For this reason, we should not expect the results of Fig. 1 [computed at the $(\pi,0)$ point] to apply at other k points such as those of Figs. 4(a)–4(c), where the relative intensities of the A and B features are seen to be generally comparable.

If the MDC's show the bilayer splitting, one would expect to see this effect in the EDC's as well. Figures 4(d) and 4(e) are illustrative in this regard. The OD sample in panel (d)

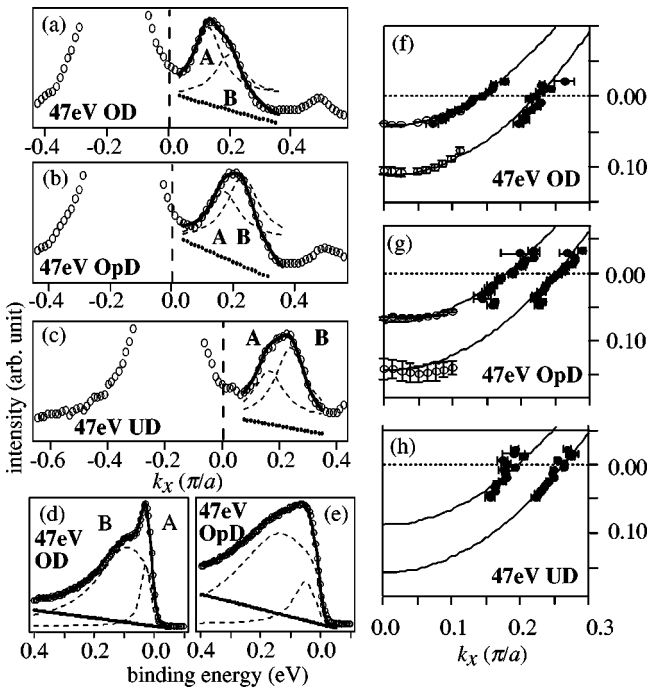

FIG. 4. Normal-state 47 eV data and corresponding fits from a cut at $k_y = 1.27\pi$ [green horizontal box of Fig. 3(h)]. The fitted region is shown by the white circle in Fig. 3(h), which only contains the primary A and B bands. (a)–(c) Overlays of MDC's at E_F with fitted curves. (d),(e): Overlays of EDC's at $(0.1\pi, 1.27\pi)$ with fitted curves. Open circles are the data, dashed lines are the associated Lorentzian peaks, dotted lines are the backgrounds, and solid lines are the overall fitting results. (f)–(h) Overlays of the centroids from EDC's (open circles) and MDC's (closed circles) with parabolic fits (solid lines).

clearly has a complicated line shape which cannot be fit with a single peak. It is highly reminiscent of the peak-dip-hump structure observed in the superconducting state and which is supposed to be due to strong-coupling effects.[20] The current data, however, are in the normal state where this structure is not supposed to exist. The current normal-state spectrum is simply characterized by a deconvolution into two peaks on top of a linear background, as shown in Fig. 4(d) (the combined spectrum was also multiplied by a Fermi-Dirac function). The OpD sample in panel (e) is also poorly fit with a single peak due to the abrupt change in slope around a binding energy of ≈ 200 meV. This again supports the scenario of two underlying features, although the uncertainty in determining peak positions becomes larger. We do not consider a similar EDC (i.e., for $k_x = 0$) for the UD sample since in that case the line shape is substantially broadened and the fitting procedure breaks down, so other cuts must be employed.

Our overall results of fitting various spectra for the three doping levels considered are compiled in Figs. 4(f)–4(h), where each set corresponds to about 20 independent fits of the type shown in panels (a)–(e). The peak centroids based on the EDC's are given by open circles, while those based on the MDC's are shown by filled circles. In either case, the error bars are indicated to show the quality of fits. The solid lines are quadratic fits which include the results of both the EDC's and the MDC's. We note that there are no obvious dispersion "kinks" present in this normal-state data, in contrast to that seen along the node in recent experiments.[21] However, our recent study focusing on this issue[23] indicates that the kinks observed near $(0,\pi)$ are of a different nature than the nodal kinks, and these $(0,\pi)$ kinks are only observed in the superconducting SC state. This lack of a kink means that there is no sharp frequency dependence to the self-energy which may shift the EDC peak positions significantly. This is consistent with the observation that the EDC and MDC peaks fall roughly on the same parabolic band.

In practice, we first fitted the lower binding-energy antibonding band A in the OD sample with a parabola and then shifted this parabola in energy to match the higher binding-energy bonding band B. Once the energy separation between these two parabolas was determined [≈ 70 meV at the momentum space location $(k_x, k_y) \approx (0.15\pi, 1.27\pi)$ for OD sample], we used these same parabolas (with their separation left unchanged) in analyzing the OpD and UD data, except for a rigid shift of both parabolas to account for the effect of doping (a shift of 30 meV was used in going from OD to OpD and of another 10 meV from OpD to UD). It is surprising that this simple procedure results in such impressive fits. It is even more surprising perhaps to see a very inert response in the size of the splitting with respect to doping. The intracell coupling $t_\perp$ as a function of $\vec{k}$ has been theoretically parametrized as $\Delta(\vec{k}) = 0.5 t_\perp [\cos(k_x a) - \cos(k_y a)]^2$, which is zero along the nodal lines and maximal at the $(\pi,0)$ points.[24] Using this simple formula to extrapolate the current data to $(\pi,0)$ we get a maximum splitting of 114 ± 8 meV or a $t_\perp \approx (57 \pm 4)$ meV, using the 47 eV data. The 22 eV data (not shown) give an estimate of $t_\perp = 54$ meV. These values are in excellent agreement with our previous estimate of 55 meV obtained using 25 eV data.[9]

We emphasize that the aforementioned parameter $t_\perp$ describes intracell hopping between adjacent CuO_2 layers in the same unit cell, and should be distinguished from the intercell hopping $t_\perp'$ between CuO_2 planes in different unit cells. Since the two hopping processes are in series, intrinsic resistivity ρ_c will be dominated by $t_\perp'$, which is the much smaller of the two. In terms of band structure, $t_\perp$ controls bilayer splitting, while $t_\perp'$ manifests itself via the more delicate *c*-axis dispersion of bands and is thus accessible in principle to ARPES experiments, although such a measurement has to date not been reported.

This study provides some insight into the doping dependencies of the resistivities ρ_{ab} and ρ_c and the nature of hopping parameters $t_\perp$ and $t_\perp'$ in Bi2212. As is well known, both ρ_{ab} and ρ_c are metallic in overdoped Bi2212, but in the underdoped regime ρ_c becomes insulating while ρ_{ab} remains metallic. These transport results have been widely taken to imply an increased 2D confinement of electrons with underdoping, whereas we find the bilayer splitting to remain at least partially coherent in the underdoped regime. The behavior of the underdoped system may nevertheless be understood by considering the case $t_\perp \geqslant \Gamma_c \gg t_\perp'$, where Γ_c is a broadening parameter (scattering rate) which describes the decoherence of states. We could then have (partially) coherent bilayer splitting (due to $t_\perp \geqslant \Gamma_c$), combined with incoher-

ent *c*-axis conductivity (due to $\Gamma_c \gg t'_\perp$), explaining both the transport data and the present ARPES results.[25] In any event, the mere observation of bilayer coupling in the optimal and underdoped regime indicates that the normal-state electronic excitations in these samples maintain some degree of coherence, even though they have widely been regarded as nonquasiparticle-like, or completely incoherent. Loss of coherence would thus appear to be a gradual process, occurring first in *c*-axis transport, then in bilayer splitting, and finally in in-plane transport. This conclusion is consistent with recent transport studies which indicate that individual bilayers in YBCO (Yttrium barium copper oxide) remain coherent across the metal-insulator transition.[26] Certainly the nature of the electronic excitations in the underdoped cuprates will remain a topic of intense discussion for a good time to come.

ACKNOWLEDGMENTS

We acknowledge sample preparation help from J. Koralek and M. Varney, a magnetometer from R. Goldfarb, and beamline support from S. Kellar, X.J. Zhou, P. Bogdanov, and Z. Hussain. This work was supported by the NSF Career Grant No. DMR-9985492, the U.S. DOE Contract Nos. DE-FG03-00ER45809 and DE-AC03-76SF00098, and has benefited from the allocation of supercomputer time at the NERSC and Northeastern University Advanced Scientific Computation Center (ASCC). The ALS and SSRL are supported by the U.S. DOE, Office of Basic Energy Sciences, and the SRC is supported by the U.S. National Science Foundation.

[1] T. Watanabe, T. Fujii, and A. Matsuda, Phys. Rev. Lett. **79**, 2113 (1997).

[2] Y. Ando, G.S. Boebinger, A. Passner, N.L. Wang, C. Geibel, and F. Steglich, Phys. Rev. Lett. **77**, 2065 (1996).

[3] E.H. Lieb and F.Y. Wu, Phys. Rev. Lett. **20**, 1445 (1968).

[4] *The Theory of Superconductivity in the High-T_c Cuprates*, edited by P. W. Anderson, Princeton Series in Physics (Princeton University Press, Princeton, NJ, 1997); S. Chakravarty, A. Sudbo, P.W. Anderson, and S. Strong, Science **261**, 337 (1993); L. Yin and S. Chakravarty, Int. J. Mod. Phys. B **10**, 805 (1996).

[5] C.M. Varma, P.B. Littlewood, S. SchmittRink, E. Abrahams, and A.E. Ruckenstein, Phys. Rev. Lett. **63**, 1996 (1989).

[6] For a review, see T. Timusk and B. Statt, Rep. Prog. Phys. **62**, 61 (1999); B. Batlogg and C. Varma, Phys. World **13**, 33 (2000).

[7] J. Orenstein and A.J. Millis, Science **288**, 468 (2000).

[8] E.W. Carlson, D. Orgad, S.A. Kivelson, and V.J. Emery, Phys. Rev. B **62**, 3422 (2000); E. Arrigoni, *ibid.* **61**, 7909 (2000); P. Kopietz, Volker Meden, and Kurt Schönhammer, Phys. Rev. Lett. **74**, 2997 (1995).

[9] Y.-D. Chuang, A.D. Gromko, A. Fedorov, Y. Aiura, K. Oka, Yoichi Ando, H. Eisaki, S.I. Uchida, and D.S. Dessau, Phys. Rev. Lett. **87**, 117002 (2001).

[10] D.L. Feng, N.P. Armitage, D.H. Lu, A. Damascelli, J.P. Hu, P. Bogdanov, A. Lanzara, F. Ronning, K.M. Shen, H. Eisaki, C. Kim, Z.-X. Shen, J.-i. Shimoyama, and K. Kishio, Phys. Rev. Lett. **86**, 5550 (2001).

[11] M.C. Asensio, J. Avila, L. Roca, A. Tejeda, G.D. Gu, M. Lindroos, R.S. Markiewicz, and A. Bansil [Phys. Rev. B **67**, 014519 (2003)] report the presence of bilayer splitting in optimally doped normal state Bi2212 at room temperature.

[12] A.A. Kordyuk, S.V. Borisenko, M.S. Golden, S. Legner, K.A. Nenkov, M. Knupfer, J. Fink, H. Berger, L. Forr, and R. Follath, Phys. Rev. B **66**, 014502 (2002)

[13] S.V. Borisenko, A.A. Kordyuk, T.K. Kim, A. Koitzsch, M. Knupfer, J. Fink, M.S. Golden, M. Eschrig, H. Berger, and R. Follath, Phys. Rev. Lett. **90**, 207001 (2003).

[14] A. Kaminski, S. Rosenkranz, H.M. Fretwell, Z.Z. Li, H. Raffy, M. Randeria, M.R. Norman, and J.C. Campuzano, Phys. Rev. Lett. **90**, 207003 (2003); T. Valla, P.D. Johnson, Z. Yusof, B. Wells, Q. Li, S.M. Loureiro, R.J. Cava, M. Mikami, Y. Mori, M. Yoshimura, and T. Sasaki, Nature (London) **417**, 627 (2002).

[15] D.L. Feng, C. Kim, H. Eisaki, D.H. Lu, A. Damascelli, K.M. Shen, F. Ronning, N.P. Armitage, N. Kaneko, M. Greven, J.-i. Shimoyama, K. Kishio, R. Yoshizaki, G.D. Gu, and Z.-X. Shen, Phys. Rev. B **65**, 220501 (2002).

[16] A. Bansil and M. Lindroos, Phys. Rev. Lett. **83**, 5154 (1999); M. Lindroos, S. Sahrakorpi, and A. Bansil, Phys. Rev. B **65**, 054514 (2002).

[17] For computational details, see Ref. 16. In Fig. 1, light is assumed to be polarized in the a-b plane. We have, however, carried out simulations for different admixtures of the out-of-plane component of the polarization vector, and find the results of Fig. 1 to be quite representative of the present experimental conditions.

[18] These may be due to the fact that we are closer to the correlated Mott state, nanoscale modulations, or intrinsic inhomogeneity. We also note that in the UD samples the bottom of the B band is at deeper energy which may add extra broadening.

[19] These are due to the 5×1 superlattice modulation along the *b* or Γ-*Y* axis.

[20] D.S. Dessau, B.O. Wells, Z.-X. Shen, W.E. Spicer, A.J. Arko, R.S. List, D.B. Mitzi, and A. Kapitulnik, Phys. Rev. Lett. **66**, 2160 (1991); J.C. Campuzano, H. Ding, M.R. Norman, H.M. Fretwell, M. Randeria, A. Kaminski, J. Mesot, T. Takeuchi, T. Sato, T. Yokoya, T. Takahashi, T. Mochiku, K. Kadowaki, P. Guptasarma, D.G. Hinks, Z. Konstantinovic, Z.Z. Li, and H. Raffy, *ibid.* **83**, 3709 (1999).

[21] A. Kaminski, M. Randeria, J.C. Campuzano, M.R. Norman, H. Fretwell, J. Mesot, T. Sato, T. Takahashi, and K. Kadowaki, Phys. Rev. Lett. **86**, 1070 (2001); A. Lanzara, P.V. Bogdanov, X.J. Zhou, S.A. Kellar, D.L. Feng, E.D. Lu, T. Yoshida, H. Elsaki, A. Fujimori, K. Kishio, J.-I. Shimoyama, T. Noda, S. Uchida, Z. Hussain, and Z.-X. Shen, Nature (London) **412**, 510 (2001); P.D. Johnson T. Valla, A.V. Fedorov, Z. Yusof, B.O. Wells, Q. Li, A.R. Moodenbaugh, G.D. Gu, N. Koshizuka, C. Kendziora, Sha Jian, and D.G. Hinks, Phys. Rev. Lett. **87**, 177007 (2001).

[22] The relative amplitudes of the A and B features cannot of course be expected to agree fully with the computations, especially in

the more correlated UD case since the calculations have been carried out in the framework of band theory. In fact, we find that there is less of a modulation with photon energy for the UD samples than for the OD samples, an effect which has also been extracted from fits in Ref. 13.

[23] A.D. Gromko, A.V. Fedorov, Y.-D. Chuang, J.D. Koralek, Y. Aiura, Y. Yamaguchi, K. Oka, Yoichi Ando, and D.S. Dessau, Phys. Rev. B **68**, 174520 (2003); A.D. Gromko, Y.-D. Chuang, A.V. Fedorov, Y. Aiura, Y. Yamaguchi, K. Oka, Yoichi Ando, and D.S. Dessau, cond-mat/0205385 (unpublished).

[24] S. Chakravarty, A. Sudbo, P.W. Anderson, and S. Strong, Science **261**, 337 (1993); O.K. Anderson, A.I. Liechtenstein, O. Jepsen, and F. Paulsen, J. Phys. Chem. Solids **56**, 1573 (1995).

[25] This would certainly be true in the limit $t'_{\perp} \rightarrow 0$.

[26] K. Semba and A. Matsuda, Phys. Rev. Lett. **86**, 496 (2001).